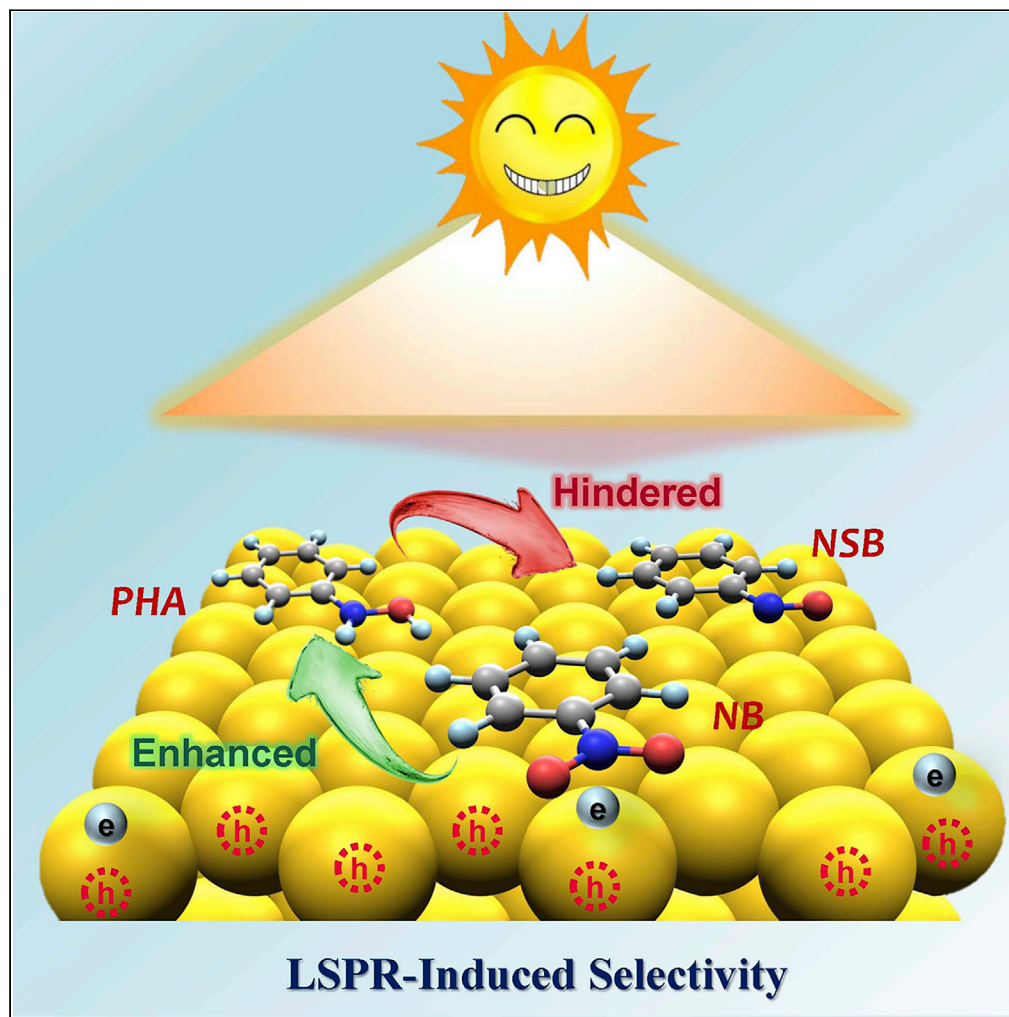## Article

Enhancing Catalytic Activity and Selectivity by Plasmon-Induced Hot Carriers

Xiao-Qing Liu, Fei-Fei Meng, Xing Chen, ..., Zhong-Qun Tian, Jian-Feng Li, Ping-Ping Fang

li@xmu.edu.cn (J.-F.L.)
fangpp3@mail.sysu.edu.cn (P.-P.F.)

HIGHLIGHTS

Hot carriers selectively accelerate the conversion rate from NB to PHA

The selectivity is ascribed to the enhanced hot electron transfer and hot holes

Light illumination leads to 1.7-time enhancement of the reduction from NB to PHA

iScience

Article

Enhancing Catalytic Activity and Selectivity by Plasmon-Induced Hot Carriers

Xiao-Qing Liu,[1,4] Fei-Fei Meng,[1,4] Xing Chen,[2] Yu-Hang Li,[3] Hao Yang,[1] Feng Peng,[3] Xi-Hong Lu,[1] Ye-Xiang Tong,[1] Zhong-Qun Tian,[2] Jian-Feng Li,[2,5,*] and Ping-Ping Fang[1,*]

SUMMARY

Plasmon-assisted chemical transformation holds great potential for solar energy conversion. However, simultaneous enhancement of reactivity and selectivity is still challenging and the mechanism remains mysterious. Herein, we elucidate the localized surface plasmon resonance (LSPR)-induced principles underlying the enhanced activity (~70%) and selectivity of photoelectrocatalytic redox of nitrobenzene (NB) on Au nanoparticles. Hot carriers selectively accelerate the conversion rate from NB to phenylhydroxylamine (PHA) by ~14% but suppress the transformation rate from PHA to nitrosobenzene (NSB) by ~13%. By adding an electron acceptor, the as-observed suppression ratio is substantially enlarged up to 43%. Our experiments, supported by *in situ* surface-enhanced Raman spectroscopy and density functional theory simulations, reveal such particular hot-carrier-induced selectivity is conjointly contributed by the accelerated hot electron transfer and the corresponding residual hot holes. This work will help expand the applications of renewable sunlight in the directional production of value-added chemicals under mild conditions.

INTRODUCTION

The efficient utilization of renewable sunlight to realize solar-chemical conversions is extremely important for modern industry because of the ever-growing energy crisis and environment problems (Aslam et al., 2018). Plasmonic metal nanostructures (e.g., Au, Ag, Cu), commonly used active catalyst with intense visible-light-absorbing properties, have attracted great attention for solar energy harvest taking advantages of a specific phenomenon defined as localized surface plasmon resonance (LSPR) (Zhang et al., 2018; Kazuma and Kim, 2019). LSPR can concentrate the far-field light radiation onto subwavelength-confined space and generate a highly energetic electromagnetic field, producing abundant highly energetic hot carriers (hot electron-hole pairs) and a great deal of local heat (ca. photothermal [PT] effect) at the metallic surface (Fang et al., 2013; Christopher and Moskovits, 2017). Because plasmonic metals inherently integrate LSPR and catalytic activities toward certain chemical reactions, their strategic incorporation into photocatalysis has been reported to be a solar-based green method with distinct advantages and promising prospects for converting simple, abundant feedstocks (e.g., water and CO_2) to value-added chemicals (e.g., hydrogen, hydrocarbons, and oxygenates) under mild conditions (Yang et al., 2016a, 2016b; Al-Zubeidi et al., 2019).

In order to unveil the underlying mechanism of LSPR-mediated chemical transformation, how to precisely distinguish the contributions of plasmon-induced hot carriers and PT effect has aroused increasing research attention recently (Zhan et al., 2018; Zhou et al., 2018; Zhang et al., 2019; Wu et al., 2019). By combining electrochemistry with surface-enhanced Raman spectroscopy (SERS), we previously established an effective method to quantitatively calculate the contribution ratio of hot carriers to the whole reactivity enhancement (Yang et al., 2015, 2016a, 2016b). Through precise quantification of the hot carrier and thermal contributions, it is manifested that hot carriers could enhance the catalytic activity by promoting either reduction reactions via hot electrons or oxidation reactions via hot holes (Jang et al., 2018; Nishi and Tatsuma, 2019; Wilson et al., 2019).

Despite the encouraging achievements made on the employment of LSPR for solar energy-based catalytic activity enhancement, how to enhance reaction selectivity via LSPR is still very challenging. Among the very
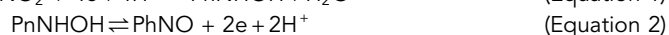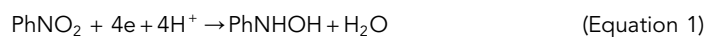
limited work reported previously, the main strategy to achieve this goal is to finely tune the excitation wavelength to adapt different reaction energy levels (Yang et al., 2016a, 2016b; Marimuthu et al., 2013). For instance, the photoexcitation of LSPR by 580-nm visible light could effectively protect Cu nanoparticles from oxidation and consequently improve the steady-state selectivity greatly in propylene epoxidation on the Cu surface (Marimuthu et al., 2013). Similar wavelength-dependent reaction pathways were also observed for the carbon dioxide hydrogenation (Zhang et al., 2017; DuChene et al., 2018; Quiroz et al., 2018; Robatjazi et al., 2017). However, present studies are mainly focused on photocatalytic reactions, whereas using LSPR to alter electrochemical reaction pathways has never been achieved before. This work represents a significant step toward understanding the respective impacts of hot carriers and PT effect on the reaction activity and selectivity, which is anticipated to give some clue for future applications of solar energy to boost the chemical transformation efficiency.

In this work, by employing the electrochemical redox of nitrobenzene (NB) on Au nanoparticles (NPs) as a model, we demonstrate the feasibility of using solar light to enhance both the reaction activity and selectivity and clearly unravel the relevant mechanism. Electrochemistry and SERS are combined to study the kinetics as a function of concentration, temperature, and illumination duration and to distinguish the respective contribution of the LSPR-induced hot carriers and PT effect. It is verified that the instant light illumination displays high catalytic selectivity, increasing the reduction of NB to phenylhydroxylamine (PHA) by ca. 14% yet suppressing the oxidation from PHA to nitrosobenzene (NSB) by ca. 13%. When H^+ is added as an electron acceptor, the oxidation course of PHA to NSB is hindered by ca. 43%, implying a hot-carriers-involved mechanism for the as-observed catalytic selectivity. In situ temperature monitoring by SERS reveals that light illumination up to 30 min can lead to a temperature rise from 23°C to 93°C right at the Au NPs surface, which can further boost the catalytic activity by 56%. This work might shed light on the employment of renewable sunlight for the directional conversion of energy-related chemicals, especially those with complex products.

RESULTS

Light-Induced Enhancement of the Catalytic Activity and Selectivity

Electrochemical characterizations toward NB were first carried out by using 55-nm Au NPs as the working electrode (Figure S1). As shown in Figures 1A and 1B, the cyclic voltammogram (CV) of NB displays two cathodic peaks (denoted as R_1 and R_2) and one anodic peak (denoted as O_1). According to the literature (Yi et al., 2007; Jayabal and Ramaraj, 2014), R_2 corresponds to the irreversible reduction of NB to PHA through four electron transfer process, whereas the O_1/R_1 couple is attributed to the reversible electrochemical redox process between PHA and NSB via two electron transfer process, as illustrated in the following equations:

$$PhNO_2 + 4e + 4H^+ \rightarrow PhNHOH + H_2O \qquad \text{(Equation 1)}$$
$$PnNHOH \rightleftharpoons PhNO + 2e + 2H^+ \qquad \text{(Equation 2)}$$

where Ph stands for the aromatic group. Such peak assignments are also confirmed by the in situ SERS tracking of the electrochemical products at different reaction stages (Figure S2). Note that the O_1/R_1 peaks only appear in the second scan segment as the reactant of O_1 (i.e., PHA) is freshly formed by R_2 in the first CV segment (from 0 to −1.0 V) (Figure S3).[21] The O_1 peak current is proportional to the PHA concentration, which positively correlates to the NB concentration. Therefore, both R_2 and O_1/R_1 couple increase with the concentration increase of the NB (Figure S4A), in accordance with the literature (Singh et al., 2012; Gupta et al., 2017). Moreover, good linear relationships are obtained between the peak current and NB concentration for all these three peaks (Figure S4B–S4D).

The light influence on catalytic performance of Au NPs is then investigated by comparing the CVs of NB with and without instant light illumination. When the incident light is instantaneously switched on, the peak current density rise of R_2 attains ca.14% (Figure 1B). In situ SERS measurements in Figure 1C reveal that NB is converted to PHA after 30 s electrolysis at −0.8 V, either with or without illumination, seeing no noticeable differences. It is thus clear that light illumination does not alter the reaction path and the as-observed peak intensity enhancement should be ascribed to the increased production of PHA molecules. Correspondingly, the peak current of O_1 is theoretically anticipated to increase since more reactants (PHA) are produced in the first stage. Surprisingly, the O_1 peak current declines slightly with instant illumination, indicating that the LSPR effect initiated by instant illumination selectively accelerates the reduction process from NB to PHA but suppresses the oxidation reaction from PHA to NSB. When the light is
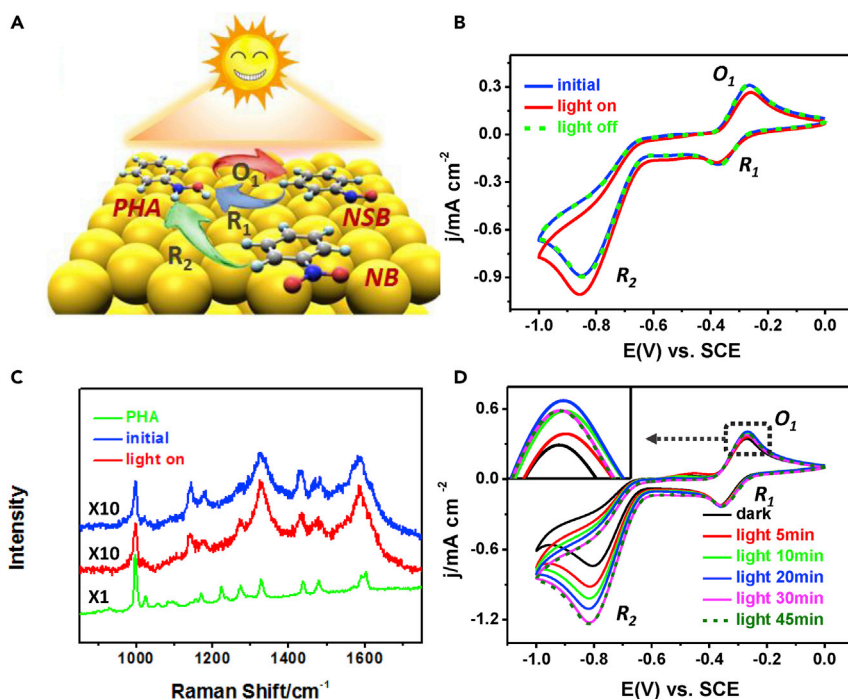
Figure 1. Light-induced enhancement of the redox processes of NB

(A) Schematic illustration of the electrochemical redox processes of NB on Au NPs.

(B) Influence of instant illumination on different processes in 2 mM NB on Au NPs.

(C) The *in situ* SERS of the electrolysis products of 2 mM NB at −0.8 V for 30 s, with (red curve) and without (blue curve) illumination.

(D) Influence of illumination time on CVs and the magnification of O_1 peak is presented in the inset. pH = 7, scan rate: 50 mV s^{-1}.

suddenly chopped, the R_2 experiences a decrease, whereas O_1 undergoes an increase, resulting in a CV curve overlapped well with the initial one (Figure 1B). In addition, further extension of light exposure duration persistently facilitates the conversion process of NB to PHA and a chemical equilibrium is achieved after 30 min continuous irradiation (Figure 1D). To be specific, peak R_2 rises gradually with the illumination time extension, keeping stable after 30 min. The O_1 process first increases and then decreases, reaching a maximum at 20 min and finally remaining constant after 30 min (Figure 1D inset).

Contributions of LSPR-Induced Photothermal Effects and Hot Carriers

To figure out the respective roles of hot carriers and PT-effect-induced local heating in LSPR-mediated NB redox processes, it is of great importance to precisely monitor the local temperature variation right at the Au NPs surface. SERS has been demonstrated to be a valid method for *in situ* detection of highly localized temperature with both high sensitivity and accuracy. Herein, we employ 4-methoxyphenyl isocyanide as the thermosensitive probe molecule because the frequency of its N≡C vibration ($v_{N≡C}$) is strongly dependent on temperature in SERS (Hu et al., 2018; Yang et al., 2015). As presented in Figure 2A, the $v_{N≡C}$ experiences a continuous blue shift with the gradual temperature rise from 20°C to 100°C, and a good linear relationship is obtained between its Raman shift and the working temperature (Figure 2B). As a consequence, the localized temperature elevation induced by illumination at the Au NPs surface could be directly read out from the work plot by measuring the $v_{N≡C}$ in SERS (Figure 2C). The Au NPs surface temperature gradually increases from 23°C, 24°C, 42°C, 57°C, 82°C, 93°C to 95°C when the illumination times are prolonged from 0, 1, 5, 10, 20, 30 to 45 min (Figure 2D). Further illumination does not obviously change the surface temperature because of the balance between the PT heating and the heat transfer. Namely, the temperature on the Au NPs almost keeps constant after 30 min illumination.

The detailed impact of light illumination on the electrochemical behavior of NB can be thus disentangled by correlating the detected localized temperature with the corresponding CV curves. Obviously, the surface temperature of Au NPs hardly changes when the light is immediately switched on, as previously
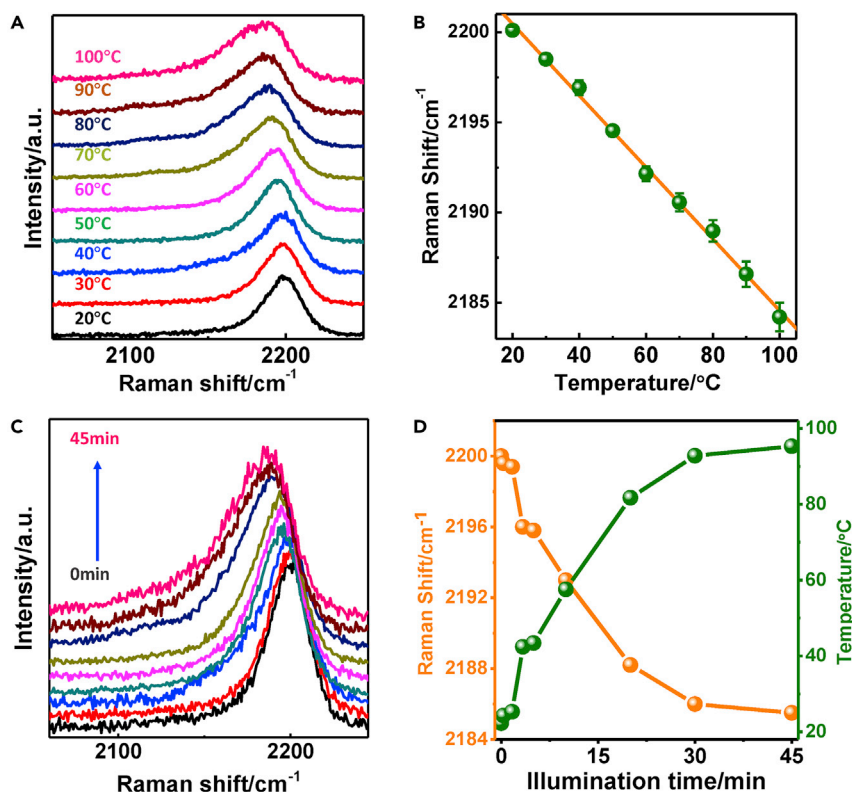
Figure 2. Detection of the surface temperature of Au NPs by SERS

(A) SERS spectra of $\nu_{N \equiv C}$ on 55 nm Au NPs obtained at a series of temperature, (B) Raman shift of the $\nu_{N \equiv C}$ as a function of temperature, (C) SERS spectra of $\nu_{N \equiv C}$ on Au NPs at different illumination durations, and (D) the corresponding detected temperatures.

observed on other Au-based SPR nanocatalysts such as Au@Pt nanorods and Au@Pd@Pt NPs.[26, 27] In this case, only hot carriers (electron-hole pairs) are generated via LSPR but the PT effect does not initiate the surface temperature increase yet. Therefore, the as-observed catalytic selectivity in Figure 1B is merely contributed by the hot carriers at the Au NPs surface. To unravel the influence of PT effect, we further analyze the CV variations with the time lapse afterward. For the R_2 peak, a continuous current density increase is observed up to 30 min illumination because of the gradual temperature rise on the Au NPs surface. For the 70% current gain of R_2 (Figure 1D), the contribution ratios of light-induced hot carriers and the PT effect are ca. 14% and ca. 56%, respectively.

When it comes to the impact of PT effect on the O_1 process, the situation becomes more complex because the reaction substrate, PHA, is freshly generated via the R_2 step (Figure S3). On the one hand, more PHA molecules are accumulated at the Au NPs surface owing to the accelerated R_2 process by illumination, which is supposed to increase the current peak of O_1. On the other hand, heat exchanges with the Au NPs gradually warm up the nearby electrolyte, speed up the mass transfer process, and thereby promote PHA molecules to diffuse away, which is expected to decrease the current peak of O_1. Therefore, the final current density is dependent on the competitive results of these two PT-induced contradictory factors. There would be a balance with the time lapse, which perfectly explains the current variation trend that the O_1 first increases and then decreases, reaching a maximum at 20 min (Figure 1D inset). Obviously, the former factor to accumulate PHA plays a leading role during the first 20 min, whereas the latter factor compelling PHA to diffuse away dominates after 20 min light exposure (when the surrounding solution is heated to be hot enough to drive the overwhelming majority of freshly produced PHA to diffuse away). The above-mentioned balance is established after 30 min when the electrode surface temperature attains ca. 93°C, as evidenced by the constant current.

Note that, different from the water bath where all the electrolyte is heated, the temperature rise initiated by PT effect is highly localized in the close vicinity of Au NPs surface instead of the whole bulk solution. The
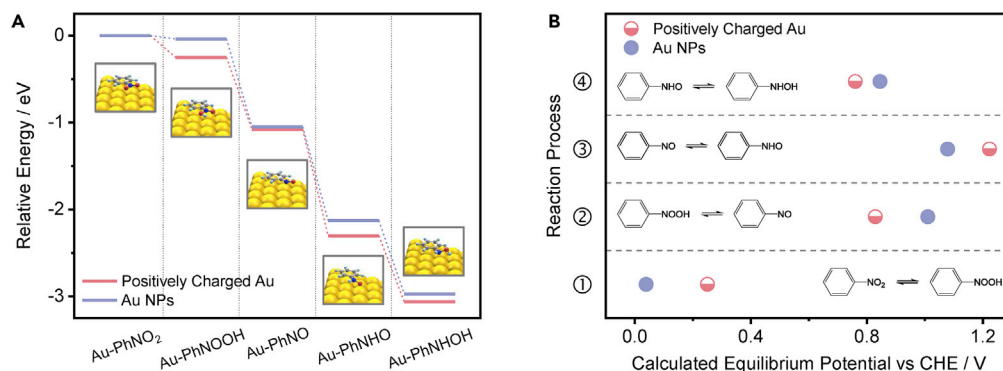
Figure 3. Theoretical simulation results
(A) Energy evolutions from Au-nitrobenzene (Au-PhNO$_2$) to Au-phenylhydroxylamine (Au-PhNHOH) in neutral and positively charged systems. (B) Corresponding calculated equilibrium potential for each elementary reaction.

specific heat capacity is 4.2 J/g for water but only 0.13 J/g for gold; therefore, the surrounding water solution is supposed to be warmed up very slowly by the "hot" Au NPs. So, the temperature rise would be localized on the Au NPs surface during the illumination, which would result in a different impact on the mass transfer courses of NB in contrast to the bulk solution temperature rise. To testify this viewpoint, we changed the temperature of the bulk solution or the scan rate to control the mass diffusion courses during the CV measurements. As the bulk electrolyte temperature increases from 30°C to 80°C, a constant decrease of O_1 peak is seen (Figure S5). When the scan rate is increased from 50 to 300 mV/s, such decrease trend is greatly suppressed, which should be attributed to the diminished diffusion of PHA at a higher scan rate (Figure S6).

So far, by virtue of *in situ* SERS sensing, we have successfully resolved the contribution ratios of light-induced hot carriers and PT effect to catalytic performance enhancement of the LSPR-mediated NB redox. The hot carrier effect can greatly enhance the selectivity, whereas the PT effect can greatly improve the catalytic activity. That is, instant illumination selectively speeds up the reduction peak R_2 but impedes the oxidation process O_1 correspondingly. However, it remains mysterious how hot carriers alter the energy barriers of relevant electrochemical reactions and lead to such unique selectivity. We further rely on density functional theory (DFT) calculations to explain the above experimental results.

Mechanism Study of the Enhanced Selectivity by DFT Calculations

There are two kinds of hot carriers on the Au NPs surface, the hot electrons and hot holes, respectively. Generally, the hot electrons generated by LSRP deviate away from the electron equilibrium state via the following two channels: (1) recombination with the holes and (2) participation in chemical reactions. In our case, to release their excessive energy, the hot electrons directly participate in the NB electroreduction, which advances the conversion rate of NB to PHA. The depletion of hot electrons by the reactants leaves plenty of hot holes (Pensa et al., 2019), making the Au NPs surface positively charged, which is testified to further strengthen the selectivity by DFT simulations.

Figure 3A presents the energy evolution from NB to PHA on both neutral and positively charged Au NPs surfaces. The positively charged state represents Au NPs with the residual hot holes while hot electrons participate in the reaction, which has been illustrated in detail in the literature.[28] In terms of the transformation from NB to PHA, the overall reaction energy barrier for positively charged Au NPs is around −3.06 eV, lower than that of Au NPs (−2.97 eV). The lower the energy barrier is, the more easily the reaction can take place. Therefore, the transformation from NB to PHA is enhanced on the positively charged Au NPs surface owing to its smaller energy barrier. Accordingly, it indicates that the positive Au sites, formed by photoexcitation, are the valid active center to further promote the reduction of NB to PHA. By comparison, for the transformation from PHA to NSB in Figure 3A, the overall reaction energy barrier for positively charged Au NPs is changed from −3.06 to −1.08 eV, exhibiting an energy barrier change of 1.98 eV. For the Au NPs, the energy barrier varies from −2.97 to −1.05 eV, showing an energy barrier change of 1.92 eV. Therefore, the positive Au site, formed by photoexcitation, hinders the transformation from PHA to NSB.
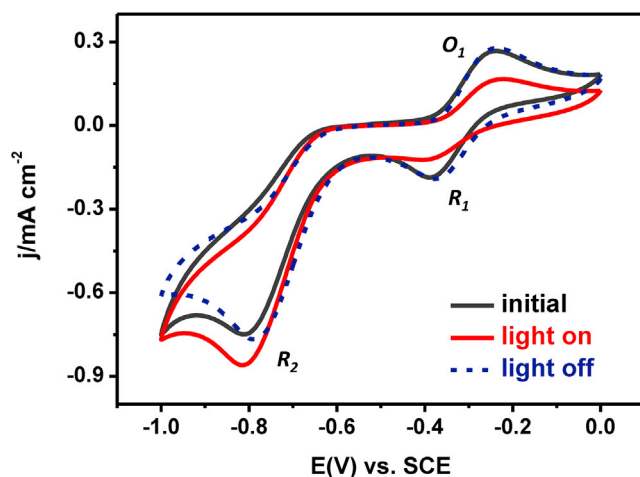
Figure 4. Light-induced enhancement of catalytic selectivity at acidic environment
Influence of illumination on CVs for Au NPs in 2 mM NB at pH = 3 at room temperature. Scan rate: 50 mV s^{-1}.

To clarify this viewpoint, we further calculate the corresponding equilibrium potential for each elementary reaction during NB redox, as presented in Figure 3B. For the reduction from NB to PHA (reaction pathway: ① → ② → ③ → ④), ① represents the potential determination step. Obviously, the positively charged Au possesses higher equilibrium potential, which makes the whole reaction much easier in contrast to Au NPs. Conversely, when the oxidation from PHA to NSB is performed (reaction pathway: ④ → ③), ③ represents the potential determination step, where the positively charged Au exhibits higher equilibrium potential, making the oxidation more difficult to take place. The DFT simulations support our experimental results and validate that the hot carriers initiate the as-observed selectivity.

Our experimental and DFT calculation results enable us to propose a plausible hot-carriers-involved mechanism for the LSPR-induced selectivity toward the electrochemical redox courses of NB. Under instant illumination, the LSPR induces the electron-hole pair separation on the Au NPs. The hot electrons transfer and participate in the transformation from NB to PHA, which facilitates the electroreduction reaction. The corresponding residual holes make the Au NPs positively charged instantly compared with the Au NPs without illumination, which further enhances the electroreduction of NB to PHA. In the case of PHA electrooxidation to NSB, the electron-hole pair separation occurs again under illumination, but the enhanced electron transfer decreases the oxidation process reaction and the corresponding residual holes that make Au NPs positively charged further hinder the reaction. Therefore, the LSPR-induced hot carriers can selectively enhance the electroreduction process of NB to PHA but suppress the electrooxidation process from PHA to NSB, in agreement with the CV in Figure 1B.

Experimental Verification of the Hot-Carriers-Involved Mechanism

To validate the reliability of the proposed mechanism, we then performed a parallel electrochemical test in acidic environment. Herein, H^{+} is employed as a competitive acceptor of hot electrons initiated by illumination. Compared with the system at pH = 7, the hot electrons can be captured more easily at pH = 3, leaving more hot holes at the electrode surface. The Au NPs thus become more positively charged, thereby facilitating the electroreduction of NB to PHA and hindering the oxidation from PHA to NSB. As illustrated in Figure 4, owing to the instant light illumination, the peak current density of R_2 increases from 0.75 to 0.88 mA cm^{-2}, whereas O1 declines from 0.28 to 0.16 mA cm^{-2}. The instant-light-on thus enhances R_2 by ca.17% (slightly higher than that at pH = 7) and suppresses O_1 by 43% (substantially higher than that at pH = 7), thereby testifying the hot-carriers-involved mechanism. As expected, such variations are completely reversible when the light is suddenly cut off, which should be attributed to the prompt dynamic of hot-carrier generation/annihilation. This work provides a new train of thoughts for finely tuning the selectivity by plasmonic hot carriers.

DISCUSSIONS

In summary, we have demonstrated that instant illumination initiates high activity and selectivity in plasmon-mediated NB redox on Au NPs, especially boosting the conversion from NB to PHA yet restricting the oxidation of PHA to NSB. At pH 7, the LSPR effect of Au NPs results in 70% conversion efficiency

enhancement from NB to PHA, in which hot carriers and PT effect account for 14% and 56%, respectively. Experimental results and DFT simulations reveal that such specific selectivity is conjointly contributed by two factors: (1) the hot electrons transfer to participate in the NB redox; (2) the hot holes left on the Au NPs surface are capable of lowering the energy barrier of the former reaction but elevating that of the latter one. Such hot-carriers-involved mechanism is further experimentally testified by the addition of H^+ as an exceptional electron acceptor. Consequently, the suppression ratio for PHA-NSB conversion is substantially enlarged from 13% to 43%. This innovative work would give an enlightening clue concerning the future wider applications of solar energy for directional chemical transformation.

Limitations of the Study

The contribution ratio of the hot carriers and PT to the reaction activity and selectivity might be highly dependent on the wavelength of the incident light for the LSPR-driven electrochemical reactions. Their relationship should be investigated in detail in the future.

Data and Code Availability

The data that support the findings of this study are available from the corresponding author upon reasonable request.

Lead contact

J. Li (li@xmu.edu.cn).

Materials Availability

All the materials necessary to reproduce this study are included in the manuscript and Supplemental Information.

METHODS

All methods can be found in the accompanying Transparent Methods supplemental file.

SUPPLEMENTAL INFORMATION

Supplemental Information can be found online at https://doi.org/10.1016/j.isci.2020.101107.

AUTHOR CONTRIBUTIONS

X.-Q.L., F.-F.M., and X.C. performed the synthetic experiments and electrochemical measurements. H.Y. performed the SERS detections. J.-F.L. and Z.-Q.T. constructed the electrochemistry and DFT calculations studies. Y.-H.L. and F.P. carried out the DFT simulations. X.-H.L. and Y.-X.T. supported with the electrochemistry studies. J.-F.L. and P.-P.F. conceived the idea and wrote the paper. All the authors participated in the data analyses and result discussions.

DECLARATION OF INTERESTS

The authors declare no conflict of interest.

REFERENCES

Al-Zubeidi, A., Hoener, B., Collins, S., Wang, W., Kirchner, S., Jebeli, S., Joplin, A., Chang, W., Link, S., and Landes, C. (2019). Hot holes assist plasmonic nanoelectrode dissolution. Nano Lett. *19*, 1301–1306.

Aslam, U., Rao, V.G., Chavez, S., and Linic, S. (2018). Catalytic conversion of solar to chemical energy on plasmonic metal nanostructures. Nat. Catal. *1*, 656–665.

Christopher, P., and Moskovits, M. (2017). Hot charge carrier transmission from plasmonic nanostructures. In Annu. Rev. Phys. Chem., *Vol 68*, M.A. Johnson and T.J. Martinez, eds., pp. 379–398.

DuChene, J., Tagliabue, G., Welch, A., Cheng, W., and Atwater, H. (2018). Hot hole collection and photoelectrochemical CO2 reduction with plasmonic Au/p-GaN photocathodes. Nano Lett. *18*, 2545–2550.

Fang, Z., Zhen, Y., Neumann, O., Polman, A., Javier Garcia de Abajo, F., Nordlander, P., and Halas, N. (2013). Evolution of light-induced vapor generation at a liquid-immersed metallic nanoparticle. Nano Lett. *13*, 1736–1742.

Gupta, R., Rastogi, P., Ganesan, V., Yadav, D., and Sonkar, P. (2017). Gold nanoparticles decorated mesoporous silica microspheres: a proficient electrochemical sensing scaffold for hydrazine and nitrobenzene. Sensor. Actuat. B Chem. *239*, 970–978.

Hu, S., Liu, B., Feng, J., Zong, C., Lin, K., Wang, X., Wu, D., and Ren, B. (2018). Quantifying surface temperature of thermoplasmonic nanostructures. J. Am. Chem. Soc. *140*, 13680–13686.

Jang, Y.J., Chung, K., Lee, J., Choi, C., Lim, J.W., and Kim, D. (2018). Plasmonic hot carriers imaging: promise and outlook. ACS Photon. *5*, 4711–4723.

Jayabal, S., and Ramaraj, R. (2014). Bimetallic Au/Ag nanorods embedded in functionalized silicate sol–gel matrix as an efficient catalyst for nitrobenzene reduction. Appl. Catal. A Gen. *470*, 369–375.

Kazuma, E., and Kim, Y. (2019). Mechanistic studies of plasmon chemistry on metal catalysts. Angew.Chem.Int. Ed. *58*, 4800–4808.

Marimuthu, A., Zhang, J.W., and Linic, S. (2013). Tuning selectivity in propylene epoxidation by plasmon mediated photo-switching of Cu oxidation state. Science *339*, 1590–1593.

Nishi, H., and Tatsuma, T. (2019). Accelerated site-selective photooxidation on Au nanoparticles via electrochemically-assisted plasmonic hole ejection. Nanoscale *11*, 19455–19461.

Pensa, E., Gargiulo, J., Lauri, A., Schlucker, S., Cortes, E., and Maier, S.A. (2019). Spectral Screening of the Energy of Hot Holes over a Particle Plasmon Resonance. Nano Lett. *19*, 1867–1874.

Quiroz, J., Barbosa, E.C.M., Araujo, T., Fiorio, J., Wang, Y., Zou, Y., Mou, T., Alves, T., de Oliveira, D., Wang, B., et al. (2018). Controlling reaction selectivity over hybrid plasmonic nanocatalysts. Nano Lett. *18*, 7289–7297.

Robatjazi, H., Zhao, H., Swearer, D., Hogan, N., Zhou, L., Alabastri, A., McClain, M., Nordlander, P., and Halas, N. (2017). Plasmon-induced selective carbon dioxide conversion on earth-abundant aluminum-cuprous oxide antenna-reactor nanoparticles. Nat. Commun. *8*, 10.

Singh, S., Devi, P., Singh, D., Jain, D., and Singla, M. (2012). Sensing behavior of silica-coated Au nanoparticles towards nitrobenzene. Gold Bull. *45*, 75–81.

Wilson, A., Mohan, V., and Jain, P. (2019). Mechanistic understanding of plasmon-enhanced electrochemistry. J. Phys. Chem. C *123*, 29360–29369.

Wu, Y., Yang, M., Ueltschi, T., Mosquera, M., Chen, Z., Schatz, G., and Van Duyne, R. (2019). SERS study of the mechanism of plasmon-driven hot electron transfer between gold nanoparticles and PCBM. J. Phys. Chem. C *123*, 29908–29915.

Yang, H., He, L.-Q., Hu, Y.-W., Lu, X., Li, G.-R., Liu, B., Ren, B., Tong, Y., and Fang, P.-P. (2015). Quantitative Detection of Photothermal and Photoelectrocatalytic Effects Induced by SPR from Au@Pt Nanoparticles. Angew. Chem. Int. Edit *54*, 11462–11466.

Yang, H., Wang, Z., Zheng, Y., He, L., Zhan, C., Lu, X., Tian, Z., Fang, P., and Tong, Y. (2016a). Tunable wavelength enhanced photoelectrochemical cells from surface plasmon resonance. J. Am. Chem. Soc. *138*, 16204–16207.

Yang, H., He, L.Q., Wang, Z.H., Zheng, Y.Y., Lu, X.H., Li, G.R., Fang, P.P., Chen, J., and Tong, Y. (2016). Surface plasmon resonance promoted photoelectrocatalyst by visible light from Au core Pd shell Pt cluster nanoparticles. Electrochim. Acta. *209*, 591–598.

Yi, Q.F., Chen, A.C., Huang, W., Zhang, J.J., Liu, X.P., Xu, G.R., and Zhou, Z.H. (2007). Titanium-supported nanoporous bimetallic Pt-Ir electrocatalysts for formic acid oxidation. Electrochem. Commun. *9*, 1513–1518.

Zhan, C., Liu, B., Huang, Y., Hu, S., Ren, B., Moskovits, M., and Tian, Z. (2018). Disentangling charge carrier from photothermal effects in plasmonic metal nanostructures. Nat. Commum. *10*, 1–8.

Zhang, X., Li, X., Zhang, D., Su, N.Q., Yang, W., Everitt, H., and Liu, J. (2017). Product selectivity in plasmonic photocatalysis for carbon dioxide hydrogenation. Nat. Commun. *8*, 1–9.

Zhang, Y., He, S., Guo, W.X., Hu, Y., Huang, J., Mulcahy, J., and Wei, W. (2018). Surface-plasmon-driven hot electron photochemistry. Chem. Rev. *118*, 2927–2954.

Zhang, Z., Zhang, C., Zheng, H., and Xu, H. (2019). Plasmon-driven catalysis on molecules and nanomaterials. Acc. Chem. Res. *52*, 2506–2515.

Zhou, L., Swearer, D., Zhang, C., Robatjazi, H., Zhao, H., Henderson, L., Dong, L., Christopher, P., Carter, E., Nordlander, P., and Halas, N. (2018). Quantifying hot carrier and thermal contributions in plasmonic photocatalysis. Science *362*, 69–72.

Supplemental Information

Enhancing Catalytic Activity and Selectivity

by Plasmon-Induced Hot Carriers

Xiao-Qing Liu, Fei-Fei Meng, Xing Chen, Yu-Hang Li, Hao Yang, Feng Peng, Xi-Hong Lu, Ye-Xiang Tong, Zhong-Qun Tian, Jian-Feng Li, and Ping-Ping Fang
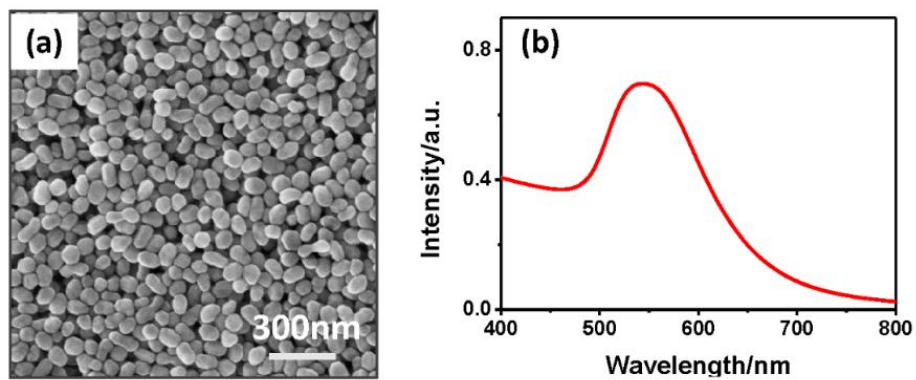
Figure S1 The scanning electron microscopy (SEM) image (a) and the UV-visible spectrum (b) of the 55 nm Au NPs. Related to Figure 1.
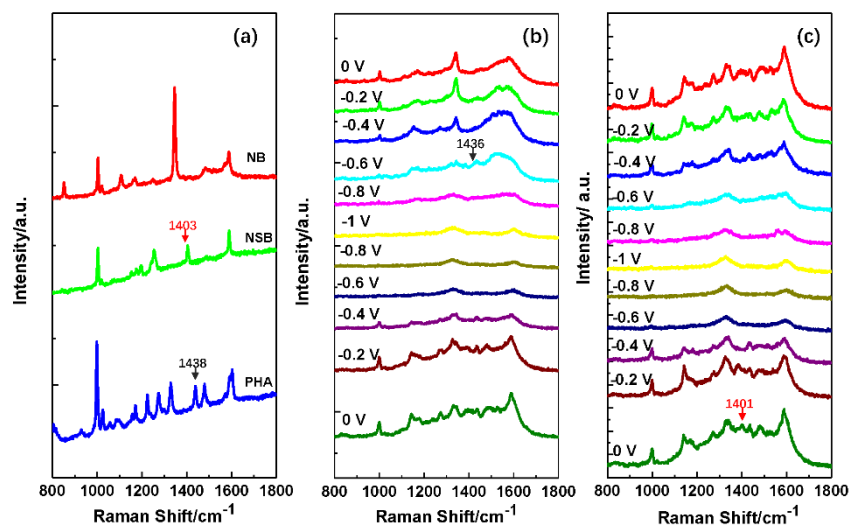
Figure S2 (a) Standard Raman spectra obtained from pure NB, NSB and PHA. *In-situ* SERS of 2 mM NB on Au NPs at different potentials; (b) the 1st CV cycle and (c) the 2nd CV cycle. The characteristic vibrations at 851, 1002, 1171, 1345, 1573 cm^{-1} belong to NB. A new band of 1436 cm^{-1} appeared at -0.6 V, indicating PHA began to form. However, when the potential went more negative than -0.8 V, most molecules except some of the protectant carbon species, would desorb from the Au NPs surface. When the potential was scanned back to -0.4 V, molecules began to adsorb on the Au NPs again. The bands of NB and PHA appeared at -0.2 V, and became more evident at 0 V. Most importantly, the bands of 1002, 1143, 1274, 1436, 1483, 1590 cm^{-1} from PHA could be clearly detected, indicating that NB was reduced to PHA. A weak band at 1401 cm^{-1} corresponding to NSB was detected at 0 V during the second CV cycle and the peak intensity was enhanced because of the accumulation of NSB. Therefore, the in-situ SERS studies validate that the NB can be reduced to PHA at -0.6 to -1 V, and the freshly formed PHA can be oxidized to NSB from -0.2 V to 0 V. Related to Figure 1.
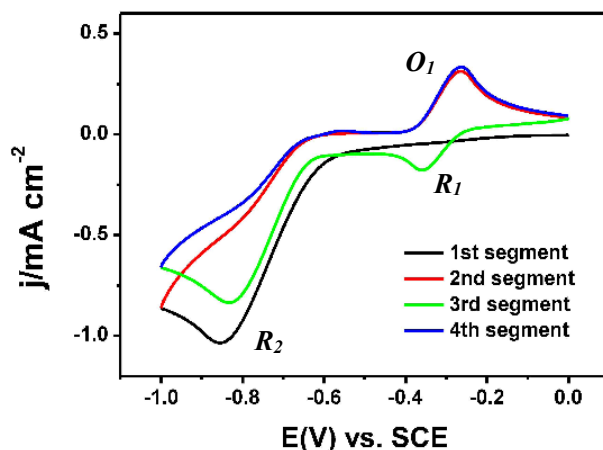
Figure S3 CVs of Au NPs in 2 mM NB; Scan rate: 50 mV s^{-1}. The PHA formed in the first segment was oxidized to NSB, and then NSB was reduced to PHA again in the third segment, which was denoted as the reversible O_1/R_1 peak in the manuscript. Related to Figure 1.
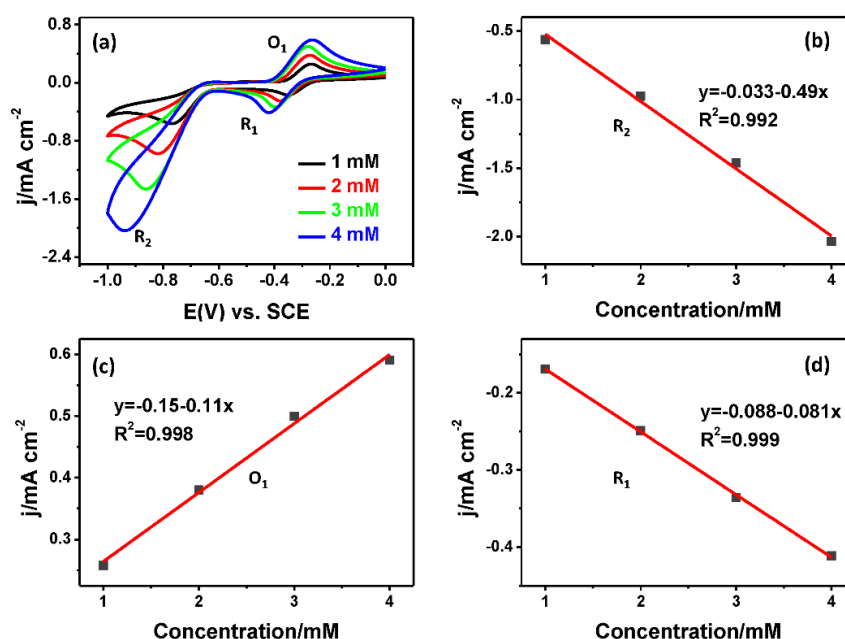

Figure S4 (a) CVs of NB with different concentrations varying from 1 mM to 4 mM. Plots of peak current versus NB concentration for R_2 (b), O_1 (c) and R_1 (d). Scan rate: 50 mV s^{-1}. Good linear relationships of the current versus concentration were obtained for R_2, O_1 and R_1, signifying a diffusion-controlled feature for all the three peaks. Related to Figure 1.
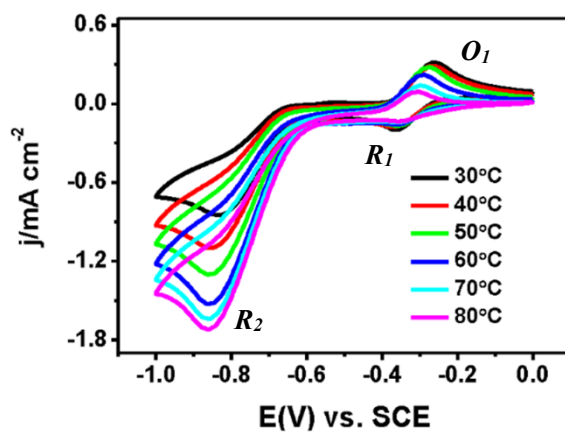
Figure S5 CVs of 2 mM NB obtained at different temperatures. Scan rate: 50 mV s^{-1}. With the gradual rise of water bath temperature up to 80 ℃, the onset potential of R_2 shifts towards more positive values and the corresponding current increases persistently owing to the boosted mass transfer courses. Similarly, for the O_1/R_1 redox process, the temperature elevation would intensify the mass transfer and the molecule diffusion in the capacitive layer. However, no supplementary reactants could fill the vacancy since PHA molecules are freshly generated by the reduction of NB. That is the reason why the peak current of O_1/R_1 continuously decreases from 30 ℃ to 80 ℃. Related to Figure 2.
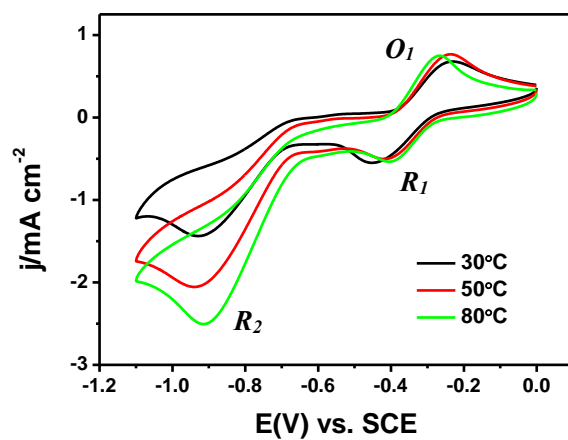
Figure S6 CVs of 2 mM NB obtained at different temperatures. Scan rate: 300 mV s^{-1}.
When the scan rate is increased from 50 to 300 mV/s, the decrease trend of the O_1/R_1
redox peaks is greatly suppressed, which should be attributed to the diminished
diffusion of PHA at higher scan rate. Related to Figure 2.

Transparent methods

Synthesis of Au NPs

All the chemicals and reagents were of analytical reagent grade and used without further purification. Millipore water was used throughout all experiments. Au NPs capped with citrate were synthesized using the classic Frens' method.[1] Specifically, 1.68 mL of 0.03 M $HAuCl_4$ (99% purity; Alfar Aesar) was added to 150 mL water in a round-bottom flask and heated to boiled. Then, 975 µL of 0.04 M trisodium citrate solution was rapidly added to the above flask with vigorous stirring, and the reaction mixture was refluxed for 40 min and kept boiling. The fluorine-doped tin oxide (FTO) glass substrates were thoroughly cleaned with ethanol, and acetone, washed by water, and then used as the substrate. Au NPs solution that ensured to cover about a monolayer of NPs on the 1 cm × 1 cm FTO pieces (20% loss was counted during the centrifugation) were centrifuged three times, dropped onto the FTO substrate and dried in vacuum oven to function as the working electrode for SERS and electrochemistry studies.

Electrochemical measurements

All the electrochemical measurements were carried out on a CHI 760e electrochemical workstation (CH Instruments, China). The electrochemical redox processes of NB dissolved in 0.1 M NaCl were characterized using a three-electrode system with a flat quartz window. A platinum plate electrode and a saturated calomel electrode (SCE) were employed as the counter and reference electrodes, respectively. Before each test, all samples were pre-saturated by N_2 to get rid of the oxygen interference. Illumination influence was investigated using a Xenon lamp as the light source (LCS-100, ORIEL, Newport) and the intensity of the incident light was always maintained at 100 mW cm^{-2} during the photoelectrochemical test. Unless stated, the CVs of NBs were acquired from 0 V to -1.0 V at 50 mV s^{-1}. The temperature control of the bulk solution was achieved by Water Bath. The neutral NB dissolved in 0.1 M NaCl was adjusted to pH=3 by adding 0.1M HCl drop by drop.

In-situ tracking of the electrochemical redox products by SERS

Raman spectra were recorded on a laser micro-Raman spectrometer (Renishaw inVia) with excitation wavelength of 632.8 nm from a He-Ne laser. In-situ tracking of the redox products of NB by SERS was realized in a specific electrochemical cell using Pt and Ag/AgCl electrodes as the counter and reference electrodes, respectively. A 3 mm-diameter glassy carbon covered by Au NPs was employed as the working electrode.

Local temperature detection on Au surface by SERS

Temperature controlled microscope systems (THMS600, Linkam Scientific Instruments Ltd.) with 10 ℃ min^{-1} of heating/freezing rates was used to control the temperature in the SERS experiments. The accuracy and stability of this system is 0.1 ℃. We choose the frequency of N≡C vibration ($\nu_{N≡C}$) of 4-methoxyphenyl isocyanide to detect the local heating of Au NPs by light illumination because the $\nu_{N≡C}$ is sensitive to the temperature. The FTO/Au substrate was immersed into 10 mM 4-methoxyphenyl isocyanide solution for 10 min to load the thermal probe and the precise temperature control was realized by the temperature controlled microscope systems. With the gradual increase of the temperature on the Au NPs, the Raman signal of $\nu_{N≡C}$ experienced a corresponding blue shift. The dependence of the $\nu_{N≡C}$ of 4-methoxyphenyl isocyanide on the temperature was plotted and the linear fit was done as the work curve. The Raman shift induced by different light irradiation times was then compared with the work curve to calculate the temperature on the hot NPs nanoparticle surface. Notably, for each sample, the SERS spectra were collected from at least 10 spots in order to average out information.

DFT calculations

DFT calculations were executed in DMol3 package (Delley, 2000).[2] The (111) facet of Au was cleaved, followed by building a (5×5×1) supercell including a vacuum

layer of 25 Å and three atomic layers of Au. All configurations were optimized with PBE functional under DNP basis set, together with the $(4 \times 4 \times 1)$ k-point set (Frens, 1973). The core treatment was DSPPs. The Tkatchenko-Scheffler method was used for DFT-D correction (Tkatchenko et al., 2009). The conductor-like screening model (COSMO) with 78.54 was employed to mimic the water solvent. In order to accelerate the SCF iteration, the electronic smearing of 7.5×10^{-4} Ha was assigned. Global orbital cutoff was set to 5.0 Å for all atoms. All calculations were spin-unrestricted. The potentials were calculated based on the computational hydrogen electrode (CHE) scheme (Norskov et al., 2004).

Supplemental References

Delley, B. (2000)From molecules to solids with the DMol(3) approach. J. Chem. Phys. 113, 7756-7764.

Frens, G. (1973) Controlled nucleation for the regulation of the particle size in monodisperse gold suspensions. Nat. Phys. Sci. 241, 20-22.

Tkatchenko, A.; Scheffler, M. (2009) Accurate Molecular Van Der Waals Interactions from Ground-State Electron Density and Free-Atom Reference Data. Phys. Rev. Lett. 102, 073005.

Norskov, J. K.; Rossmeisl, J.; Logadottir, A.; Lindqvist, L.; Kitchin, J. R.; Bligaard, T.; Jonsson, H.(2004) Origin of the overpotential for oxygen reduction at a fuel-cell cathode. J. Phys. Chem. B 108, 17886-17892.